Article history: Received 1 February 2024, last revised 28 March 2024, accepted 5 May 2024



ENHANCEMENT OF HEAT TRANSFER NUMERICALLY BY INSERTING HELICAL COILED WIRE INSIDE TUBE FLOW

Murtadha A. Hanoon¹, Mohsen H. Fagr², and Kamaal S. Mekki³

- ¹ Department of Mechanical Engineering, College of Engineering, University of Thi-Qar, Thi-Qar, 64001, Iraq. Email: murtadha.a.h@utq.edu.iq; 3.murtadha@gmail.com
- ² Department of Mechanical Engineering, College of Engineering, University of Thi-Qar, Thi-Qar, 64001, Iraq. Email: mohsenfagr@utq.edu.iq
- ³ Department of Mechanical Engineering, College of Engineering, University of Thi-Qar, Thi-Qar, 64001, Iraq. Email: Kamal-s@utq.edu.iq

https://doi.org/10.30572/2018/KJE/160301

ABSTRACT

In this numerical investigation, the effectiveness of utilizing advanced helical coiled wires (HCWs) as a tube insert for the purpose of heat transfer and turbulence enhancement under turbulent flow conditions (Reynolds numbers: 3000-11000) was examined. HCW followed a helical guide path instead of a straight one in a typical coiled wire case, resulting in increased flow complexity, six models were tested with pitch ratio (P/D) of 1, coiled wire pitch (p) of 6 mm, large base radius (R1) ranged 7-10 mm, coiled wire centerline radius (r) ranged 3-6 mm. ANSYS Fluent 22 was used for simulation. The working fluid considered throughout the study was air as a single phase flow case. The governing equations; The equation of continuity, Equations of momentum conservation, and The equation for energy conservation were solved using finite volume method and k-ɛ turbulence model. Results indicated increased Nusselt number (Nu) and friction factor (f) compared to the plain tube. Thermal performance factor (TPF) showed an inverse relationship with Reynolds number. The study reported that the circular wire without tapering insert at Re = 3000 exhibited the highest thermal performance factor of 1.228, while the highest enhancement ratio for Nusselt number of 3.86 was recorded in the same case. Also, this model recorded the maximum friction factor increasing at a friction factor ratio of 30.97.

KEYWORDS

Computational fluid dynamics; Forced convection; Heat transfer enhancement; Helical coiled wire; Heat exchanger design.



1. INTRODUCTION

Heat transfer is an essential process that holds a crucial role in diverse industrial, engineering, and scientific applications. It refers to the process of thermal energy transfer from one region to another due to a temperature difference. Understanding and optimizing heat transfer mechanisms are essential for designing efficient systems and devices. The three primary forms of heat transfer are radiation, convection, and conduction. Although each mode has importance, convection is especially noteworthy because of its broad applicability and influence on real-world situations. This mode of heat transfer is of paramount importance in numerous applications, such as industrial cooling processes (Wang & Zhang, 2023), thermal management in electronic devices (Dhumal et al., 2023), aerospace propulsion systems (Oehlschlaeger, 2022), and even natural phenomena like weather patterns and ocean currents (Bochenek & Ustrnul, 2022). The efficiency of convective heat transfer directly influences the performance and energy consumption of these systems.

Heat exchangers (HEs) are devices that transfer heat between two or more fluids. The heat transfer occurs through the process of convection in each fluid and conduction through the wall separating the two fluids. The efficacy of these heat exchangers plays a pivotal role in determining the overall efficiency of the associated systems. Enhancing the performance of HEs offers manifold advantages, including compact design, cost-effectiveness in both manufacturing and operation and energy conservation. Consequently, investigating methods to augment heat transfer has garnered significant attention among researchers (Ghassan Fadhil Smaisim, 2018).

Incorporating turbulence flow generators stands out as an effective approach for enhancing composite velocity and optimizing heat transfer within heat exchanger tubes. These generators serve to disrupt the thermal boundary layer, and amplifying tangential and radial turbulent fluctuations. Among the various turbulence flow generators, Coiled Wires (CWs) stand out as an effective means to induce swirl or turbulence near the tube wall, this led to more efficient fluid mixing between the near-wall and core regions, resulting in an enhanced heat transfer process. The unique geometric configuration of helical wire inserts generates vortices, swirls, and secondary flows within the fluid trajectory as it passes over the inserts. This phenomenon facilitates intensified fluid mixing and heightened interaction between the fluid and tube walls, thereby leading to elevated heat transfer coefficient. The literature delved into the significance of coiled wire inserts as a crucial passive heat transfer enhancement technique, garnering attention in thermal engineering research over recent decades. Researchers aim to optimize designs, facilitating the development of more efficient and compact heat exchanger systems.

(García et al., 2012) compared the thermal-hydraulic behavior of corrugated tubes, dimpled tubes, and wire coils. Wire coils were identified as the optimal choice for Reynolds numbers between 200 and 2000 in heat exchangers. (Chang et al., 2015) investigated the impacts of grooved square wire coils, illustrating enhancements in both heat transfer and thermal performance in comparison to tubes with smooth-coil tubes. (San et al., 2015) conducted an experimental analysis on thermo-hydraulic characteristics within a system incorporating a coiled wire insert, highlighting the significance of the wire diameter to tube diameter ratio and the coil pitch to tube inner diameter ratio. (Sharafeldeen et al., 2016) studied the effect of wire coil insertion in a smooth tube under constant heat flux and variable Reynolds numbers, revealing significant increases in heat transfer and friction factor. (Du et al., 2018) experimentally studied the effect of regularly spaced wire coils with a conical shape inside traverse corrugated tubes, noting increased friction factor and heat transfer. (Zimparov et al., 2022) explored the effect of the pitch of the inserted coiled wire on the heat exchanger performance experimentally, identifying the greatest benefits with a pitch of p/e = 10.0. The impact of a square cross-sectional wire inserted into a circular plain pipe on the thermohydraulic characteristics of the flow field was studied numerically by (Hinge & Patwardhan, 2019), the findings indicated that rising turbulence and velocity levels led to rising heat transfer coefficients. (Yu et al., 2020) investigated wire coils with different cross-sectional shapes in a twisted oval tube through numerical simulation, revealing enhanced heat transfer and increased pump consumption. (Sharifi et al., 2020) investigated the application of artificial neural networks and genetic algorithms to anticipate the values of heat transfer and pressure drop of tubes with wire coils under non-isothermal conditions. (Yang et al., 2021) investigated wire coil inserts in annular channels for molten salt heat exchangers, indicating significant heat transfer enhancement with proposed correlations for friction factor and Nusselt number. (Göksu & Yılmaz, 2021) employed numerical simulations to study the impact of various wire coil geometries and pitch ratios on heat transfer and pressure drop in a square duct. (Dang & Wang, 2021) explored a new twined coil insert to enhance heat transfer in a tube through numerical analysis and experiments, presenting correlations for Nusselt number and friction factor. A numerical investigation was conducted by (Aldawi, 2022) to analyse the thermal and frictional properties of a flat coil tube with spring inserts, emphasizing the enhanced heat transfer performance while taking into account the pressure drop. (García et al., 2023) explored the efficacy of wire-coils in enhancing heat transfer at low Reynolds numbers. A novel methodology based on TSP (Transition Shape Parameter) predicted friction coefficient evolution and extended transitional flow regions. Results from harp-type solar collectors

indicated that wire-coil geometries with lower ReCL values significantly enhanced heat transfer, offering potential absorber temperature reductions of up to 15%. The findings underscored the importance of selecting wire-coil geometries that aligned with applicationspecific Reynolds number ranges for optimal thermal performance and minimal pressure losses. (Kumar et al., 2023) investigated the impact of coiled spring turbulators on heat transfer and pressure drop in a triple tube heat exchanger using water and CuO/water (0.8%vol/vol) as working fluids. Results showed that lower-pitched inserts combined with CuO nanofluid achieved the highest heat transfer enhancement, especially in counter flow arrangements. Notably, at Re = 4000, the heat transfer coefficient for the lower pitch spring insert with CuO nanofluid was 144.74% higher than that of the plain tube with water. In counter flow, the Nusselt number augmentation for the triple tube with lower spring pitch and CuO nanofluid was 63.33% higher compared to the plain triple tube with water. The maximum thermal performance value was observed in the plain tube with CuO nanofluid, reaching 1.04 at Re = 4000. Furthermore, thermal performance enhancement was greater in counter flow arrangements compared to parallel flow configurations. Turbulent flow within a parabolic solar collector tube equipped with two spring insert samples of varying pitch ratios (P/D = 0.22, 0.44) and a specific cross-section was studied and simulated by (Yin et al., 2023), Cu--Fe₃O₄/Water hybrid nanofluid with volume fractions of $\varphi = 1\%$, 3%, and 5% was analysed across Reynolds numbers of 7000, 9000, and 11000. Results indicated that decreasing the pitch ratio led to increased Nusselt number and solar collector efficiency, with maximum efficiency observed at P/D = 0.22 (Re = 7000, $\varphi = 1\%$). The Field Synergy Principle highlighted the positive impact of the spring insert on heat transfer rate and solar collector efficiency. Lower pitch ratios were recommended for optimal solar collector efficiency. (Keklikcioglu & Ozceyhan, 2022) analysed the effects of using convergent, convergent-divergent, and divergent conical wire coils in ethylene glycol and water mixture flow regions on heat transfer augmentation. Three different volumetric ratios of ethylene glycol and water were investigated, along with two pitch ratios for the wire coils. Results showed that conical wire coils enhanced heat transfer rate and increased fluid friction, with the highest Nusselt number achieved with a divergent coil at a (40:60) volumetric ratio. New correlations were proposed to predict Nusselt number and friction factor, suggesting potential for improving thermohydraulic performance in engineering applications. Key conclusions included the effectiveness of ethylene glycol dispersion in water for varying temperature conditions and the significant impact of pitch ratio on heat transfer and pressure drop. The study underscored the potential of conical wire coils as an economical solution for enhancing heat transfer in thermal systems. In summary, the literature review synthesized findings from both experimental and numerical studies, providing a comprehensive understanding of the effectiveness of wire coil inserts in enhancing heat transfer. It identified gaps in research, such as the absence of studies on helical coiled wire with circular cross-sections. The present investigation endeavors to address a portion of the existing knowledge gap in this field by investigate the enhancement of heat transfer and turbulence in tube flows through the utilization of helical coiled wire inserts. Specifically, the study aims to comprehensively analyze the thermal performance and flow characteristics associated with the insertion of circular wire cross-sections into the test tube. By conducting a systematic examination, this research seeks to contribute to the advancement of knowledge in thermal engineering and fluid dynamics, particularly in optimizing heat transfer processes within industrial and engineering applications. The study plan is to develop a numerical model using computational fluid dynamics (CFD) software, ANSYS Fluent, to simulate the flow and heat transfer phenomena.

2. MODELING APPROACH AND METHODOLOGY

2.1. Physical modeling

The present study proposed a helical coiled wire (HCW) geometry as an inserted device. It offers a higher level of complexity and accordingly higher level of turbulence compared to the typical helical wire arrangement. This geometry consists of a helical wire that is coiled around a secondary helical path, which serves as a virtual guide path. The guide path plays an essential role in defining the helical coiled wire and tapered helical coiled wire (HCW-T) geometries, in turn, it can be defined by the helical line that tangents at all points to the surface of a hypothetical cylinder with base radius is R1 in the case of HCW, or in the more general case HCW-T, it is the helical line tangents at all points to the surface of a hypothetical truncated cone with large base and small base radii are R1 and R2, respectively. Fig. 1. depicts a schematic diagram for a guide path contained in a truncated cone and helical coiled wire geometry parameters fitted into a plain tube of length (L), diameter (D), and the clearance between the wire and the surface of the tube (S). HCW-T can be described by a number of dimensions, which are; guide path pitch (P), coiled wire pitch (p), large base radius (R1), small base radius (R2), coiled wire centerline radius (r), and wire diameter (e).

The proposed HCW-T geometry stands as a more encompassing form of the typical helical wire arrangement, by allowing the pitch value (P) of the guide path to tend towards infinity, and R2=R1=0, the geometry seamlessly transformed into typical helical wire configuration without

tapering. One type of HCW-T was used in this study, that is tapered decrease helical coiled wire (HCW-TD), formulated when the large base radius R1 is located in the flow inlet region.

The studied cases were simulated in the physical model with the assistance of ANSYS DesignModeler, while ANSYS SpaceClaim was used for some illustrative graphics schemes. The circular tube was a stationary, horizontal installation, 30 mm in diameter and 500 mm in length. Wire diameter is of (e = 2 mm). The clearance (S=1mm) for all models.

In the present study, the dimensionless quantity defined as pitch ratio (P/D) emerges as a critical factor shaping the geometry of tested models. This parameter defines the relationship between the pitch length (P) of the guide path and the tube diameter (D). Three pitch ratios of 1, 1.5, and 2 were used, resulting from the pitches (P) values of 30mm, 45mm, and 60mm. Another important non-dimensional quantity that is described tapered helical coiled wire geometry in the present study is the taper ratio (TR= R2/R1), defined as the ratio of the small base radius (R2) to the large base radius (R1), all tested tapered models have the same tapered ratio of (TR = 0.21). The values of large base radius (R1) were 7 mm, 8 mm, and 10 mm, and the coiled wire pitch (p) was maintained constant at 6 mm.

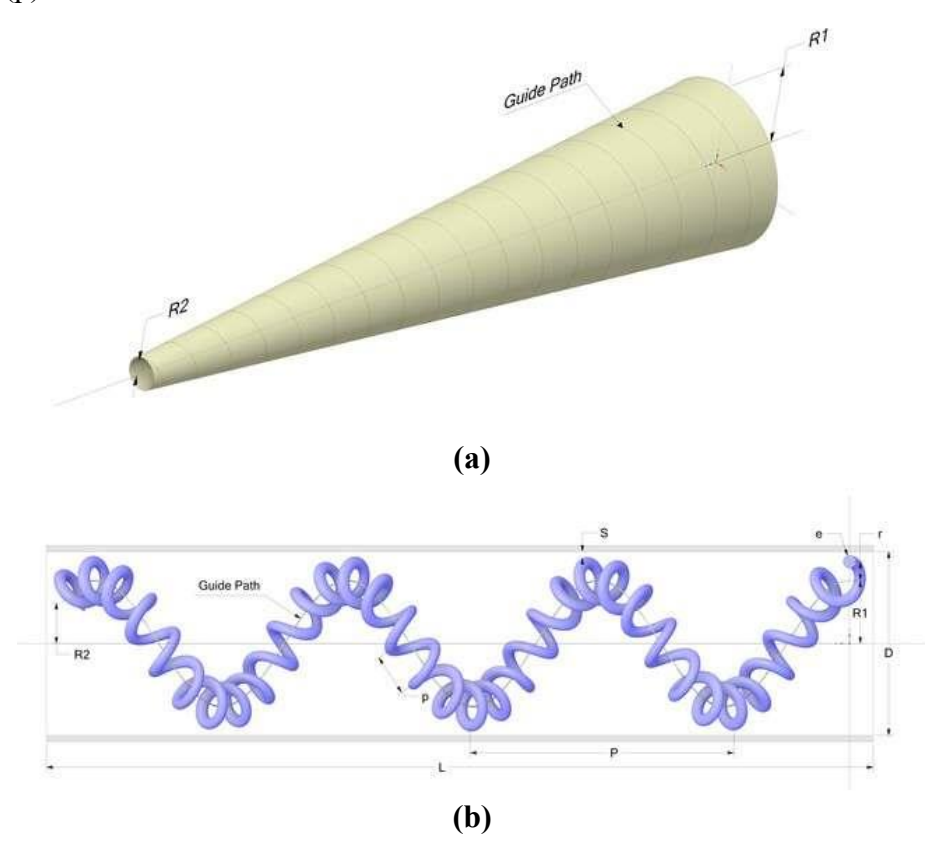


Fig. 1. (a) Conical representative of the guide path; (b) helical coiled wire geometry parameters.

The models were named according to the following pattern:

Where the field (XXXX-XX) denoted the model's abbreviation.

No.		P/D	R1 mm	r mm	p mm
1	CHCW-NT 7	1	7	6	6
2	CHCW-TD_7	1	7	6	6
3	CHCW-NT 8	1	8	5	6
4	CHCW-TD 8	1	8	5	6
5	CHCW-NT 10	1	10	3	6
6	CHCW-TD_10	1	10	3	6

Table 1. Names and dimensions of the tested models

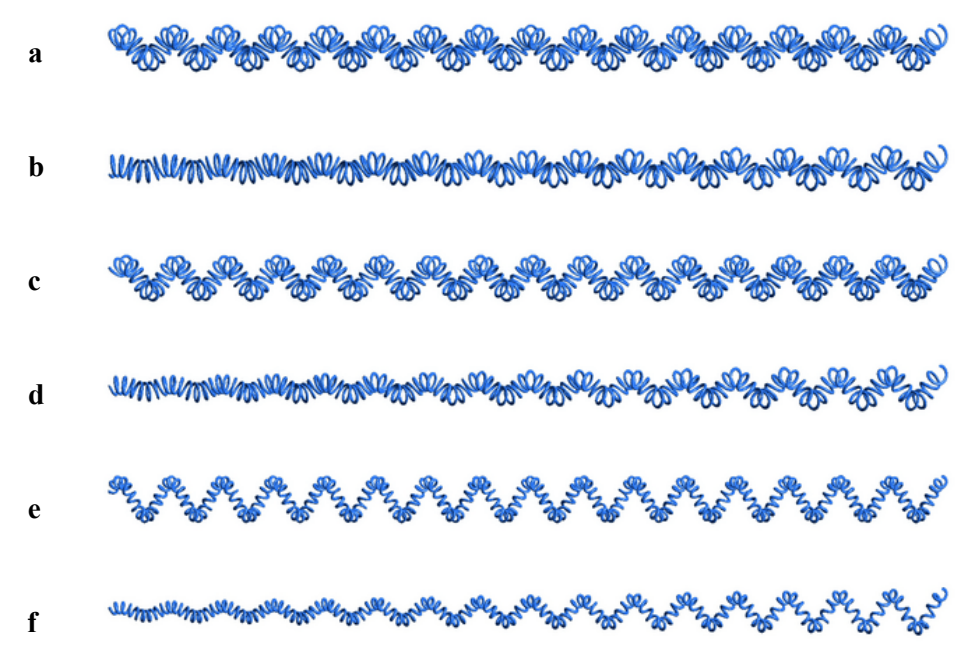


Fig. 2. Helical coiled wires of different configurations; a- CHCW-NT_7, b- CHCW-TD_7, c- CHCW-NT_8, d- CHCW-TD_8, e- CHCW-NT_10, f- CHCW-TD_10.

The impact of CHCWs was examined in this study using six different models. These models were designed to explore various configurations with different values of (R1) with and without tapering, Table 1. provides the names and dimensions of these models. The different HCWs configurations that were studied in the current investigation are shown in Fig. 2.

The tool of choice for executing simulations and computations in this study was ANSYS 22R1. The central processing unit (CPU) that powered the simulations was the Intel® Core™ i9-13900KF Processor BOX. This high-end CPU, with its 24 cores, is renowned for its exceptional performance in executing intensive tasks. Notably, ANSYS Fluent, the software used for the simulations, can effectively utilize up to 32 to 48 physical cores per dual-socket node, and even more with certain configurations. This makes the chosen CPU an excellent fit for the computational demands of this work. This was paired with the ASUS ROG Strix Z690-F Gaming DDR5 WIFI motherboard, a reliable platform that ensured optimal operation of all components. The graphics processing unit (GPU) used was the NVIDIA GeForce RTX 3060 12GB, a powerful GPU capable of rendering complex graphics and assisting in computation-

heavy tasks. The system was equipped with Kingston HyperX Fury Beast RGB DDR5 64GB 16GBx4 6000 RAM, providing ample memory for efficient data processing. Storage was handled by the Predator GM7000 PCIe 4.0 7400/6800MB/s 2TB SSD M.2 NVME, offering high-speed data access and ample space for storing large datasets.

2.2. Governing equations and boundary conditions

In the computational simulations carried out in the present investigation, various flow assumptions have been taken into account, with the working fluid being air, the flow is assumed to be three-dimensional, steady-state, turbulent, and incompressible. Additionally, the neglect of body forces, thermal radiation, and natural convection is incorporated into the simulation model. The assumed thermo-physical characteristics of the fluid remain constant with temperature, specified as ($\rho = 1.225 \text{ kg/m}^3$, $\mu = 1.789 \times 10^{-5} \text{ kg/(m·s)}$, Cp = 1006.43 J/kg·K, and K = 0.0242 W/m·K). The thickness of the tube wall is considered negligibly small. The concise expressions for the governing equations, represented by Eqs. 1-5, can be generally formulated as follows:

The equation of continuity:

$$\frac{\partial u}{\partial x} + \frac{\partial v}{\partial y} + \frac{\partial w}{\partial z} = 0 \tag{1}$$

Equations of momentum:

Momentum along the X-axis:

$$\rho \left(u \frac{\partial u}{\partial x} + v \frac{\partial u}{\partial y} + w \frac{\partial u}{\partial z} \right) = -\frac{\partial p}{\partial x} + \mu \left(\frac{\partial^2 u}{\partial x^2} + \frac{\partial^2 u}{\partial y^2} + \frac{\partial^2 u}{\partial z^2} \right)$$
(2)

Momentum along the Y-axis:

$$\rho \left(u \frac{\partial v}{\partial x} + v \frac{\partial v}{\partial y} + w \frac{\partial v}{\partial z} \right) = -\frac{\partial p}{\partial y} + \mu \left(\frac{\partial^2 v}{\partial x^2} + \frac{\partial^2 v}{\partial y^2} + \frac{\partial^2 v}{\partial z^2} \right)$$
(3)

Momentum along the Z-axis:

$$\rho \left(u \frac{\partial w}{\partial x} + v \frac{\partial w}{\partial y} + w \frac{\partial w}{\partial z} \right) = -\frac{\partial p}{\partial z} + \mu \left(\frac{\partial^2 w}{\partial x^2} + \frac{\partial^2 w}{\partial y^2} + \frac{\partial^2 w}{\partial z^2} \right)$$
(4)

The equation for energy conservation:

$$\rho C_p \left(u \frac{\partial T}{\partial x} + v \frac{\partial T}{\partial y} + w \frac{\partial T}{\partial z} \right) = K_f \left(\frac{\partial^2 T}{\partial x^2} + \frac{\partial^2 T}{\partial y^2} + \frac{\partial^2 T}{\partial z^2} \right)$$
 (5)

The boundary conditions used for solving the governing equations were for tube; stationary wall boundary condition, tube wall was exposed to a constant heat flux of (1500 W/m²), constant temperature at the inlet of (298 K), uniform velocity at the inlet of the value corresponding to Reynold numbers of 3000, 5000, 7000, 9000, and 11000, and zero-pressure

gauge is used to apply the pressure outlet condition. For helical coiled wire; stationary wall, negligible conduction heat transfer through the wire.

2.3. Numerical approaches, mesh Generation, and validation procedures

The Navier-Stokes and energy equations with boundary condition equations are solved using a computational fluid dynamics code (ANSYS FLUENT 22) based on finite volume methods. For pressure-velocity coupling, the SIMPLE method is employed, which is extensively utilized in numerical modeling of heat exchangers. By utilizing a link between velocity and pressure adjustments, this technique retrieves the pressure field while enforcing mass conservation. A second-order upwind technique was used to spatially discretize the momentum and energy equations, and a least squares cell-based gradient was employed. With a second-order spatial discretization of pressure, the velocity formulation was absolute. To attain second-order precision, the amounts of all cells were calculated using a multi-dimensional linear reconstruction technique. The governing equations with boundary conditions were solved using the pressure-based solver. The study employs the Standard k-ε Turbulence Model to accurately simulate turbulent flow behavior within the plain tube and the tube fitted with helical coiled wire inserts. The initialization of the standard solution was calculated from the inlet. For continuity and velocities, the convergence requirement was (1x10⁻⁵) for the absolute criteria of residual, while for energy, the highest value of the absolute criteria was (1 x 10⁻⁶).

In the context of simulation, mesh generation assumes a critical role, significantly influencing the precision and reliability of computational results. The process of spatial discretization within the computational domain commences with mesh construction, dividing the physical space into discrete parts or cells. This foundational step directly impacts the simulation's ability to study and depict underlying physical processes effectively. Beyond ensuring an accurate representation of domain geometry, a well-constructed mesh facilitates the application of governing equations and conservation laws. Consequently, simulations can precisely capture fine system characteristics and govern multiple spatial scales, all made possible by meticulously generated meshes (Hussien et al., 2023). In the present work, the 3D domains of studied cases were divided using hybrid mesh because of the complexity of these flow domains. The meshing steps in Workbench, ANSYS 22 by using Fluent With Fluent Meshing were utilized to get the meshes of the studied cases. The generated mesh for the studied case of tubes fitted with CHCW, are shown, in Fig. 3.

To confirm the grid independence of the performed numerical simulations, the grid refinement process was evaluated for each case under study by segmenting the domain into various grids

and comparing the outcomes of the friction factor and Nusselt number.

The associations between the friction factor, Nusselt number, and number of grid elements for the chosen case are shown in Fig. 4. As indicated in this figure, the difference between the results obtained from successive grids diminishes with finer grids, reflecting the convergence of these results. In all the cases examined, a deviation of less than 2% in both the friction factor and the Nusselt number is deemed acceptable for choosing a grid that will yield stable and grid-independent results. The reduction in deviation when using finer meshes is due to a decrease in the errors associated with applying the governing equations, which is a result of the reduced intervals of these equations' applications. Given the chosen constraint of a deviation in the results, the specific grid for each case is presented in Table 2. For each specified Reynolds number, the average computational cost for performing a simulation, except that for the plain tube, was typically between 4 and 5 hours.

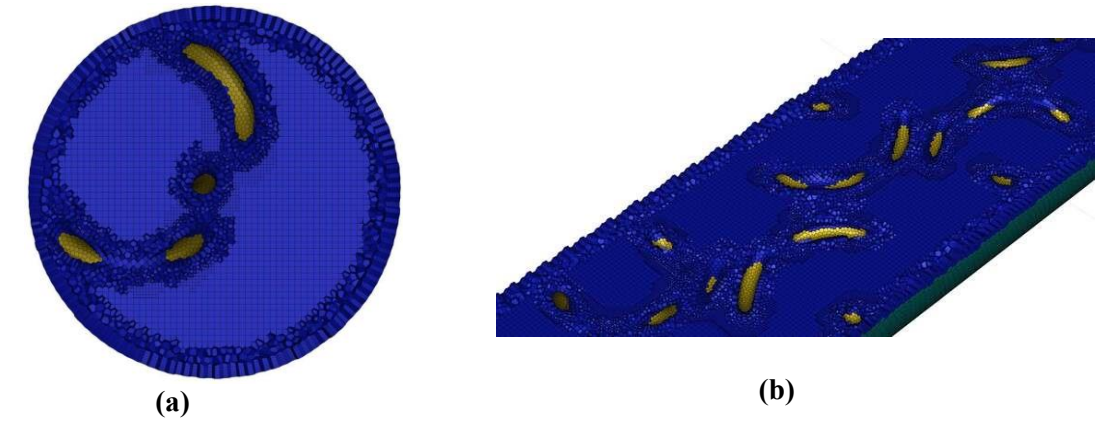


Fig. 3. Generated mesh of hybrid elements (poly-hexacore) of tube fitted with CHCW; (a) Cross-section (b) three-dimensional view.

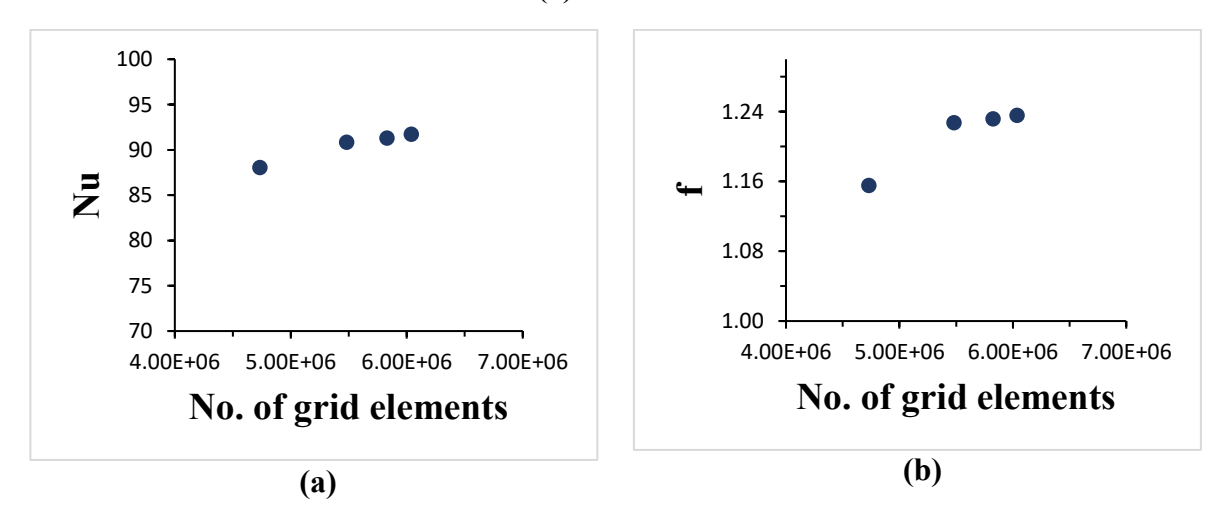


Fig. 4. Computed outcomes for a tube equipped with the THCW-NT_7 configuration under varying grid densities at Re = 7000 for; (a) Nusselt number, and (b) the friction factor.

Given the lack of open-access researches on the use of helical coiled wire as an insert for enhancing thermo-hydraulic performance, it was necessary to conduct a validation study with typical circular helical wires, as well as with plain tube. Consequently, a new model of a typical circular helical wire was developed. This model was designed to be consistent with the validated model and was tested under identical simulation conditions to that for the main models.

		1 8
No.	Name	Grid elements
1	PT	189,437
2	CHCW-NT_7	6,039,010
3	CHCW-TD_7	4,437,444
4	CHCW-NT_8	5,819,385
5	CHCW-TD_8	4,199,708
6	CHCW-NT_10	5,242,005
7	CHCW-TD 10	4 115 673

Table 2. The studied cases and their specified grids.

The numerical outcomes for the Nusselt number and Darcy friction factor, both for a plain tube and tubes fitted with typical circular helical wires, were compared with findings from established studies (Abd zaid & Hamzah, 2021). This comparison was conducted to confirm the validity and acceptability of the results obtained in this work.

The Nusselt numbers obtained from the plain tube were evaluated against the Gnielinski correlation (Dostál et al., 2022). For Reynolds numbers Re = 9000 and 11000, the Dittus-Boelter correlation (Taler, 2017) was used for comparison. The obtained friction factor results from the plain tube were compared with the correlations presented by Petukhov and Blasius (Taler, 2017).

The outcomes for the Nusselt number and friction factor, resulting from the tube equipped with a typical circular helical wire in this study, were compared with the correlations found in the experimental research conducted by (Sharafeldeen et al., 2016).

As depicted in Fig. 5., the theoretical Nusselt number for the plain tube is validated. The numerical outcomes of the current study align with prior research, exhibiting an average deviation of 7.8% with the Gnielinski correlation along the whole Reynolds number range examined in this study. Furthermore, a minimal deviation of 0.7% was observed when compared with the Dittus-Boelter correlation for Reynolds numbers greater than or equal to 9,000.

In Fig. 6., the validation of the theoretical friction factor results for the plain tube, as derived in the present study, is depicted. It is discernible that the numerical friction factor outcomes exhibit a noteworthy level of agreement with the prior investigations conducted by Petukhov and Blasius. The comparative analysis reveals that the average deviation amounts to 4.2% and 2.4%, respectively.

Fig. 7. validates the theoretical Nusselt number results derived in this study for a tube equipped with a typical circular helical wire. The numerical outcomes were consisted with previous research, showed an average deviation of 9.1% when compared with the correlation from the study conducted by Sharafeldeen, MA, et al. Fig. 8. provides validation for the theoretical friction factor results that were obtained in this study for a tube fitted with a typical circular helical wire. The numerical outcomes demonstrated an average deviation of 9.7% when compared with the correlation from the study conducted by Sharafeldeen, MA, et al.

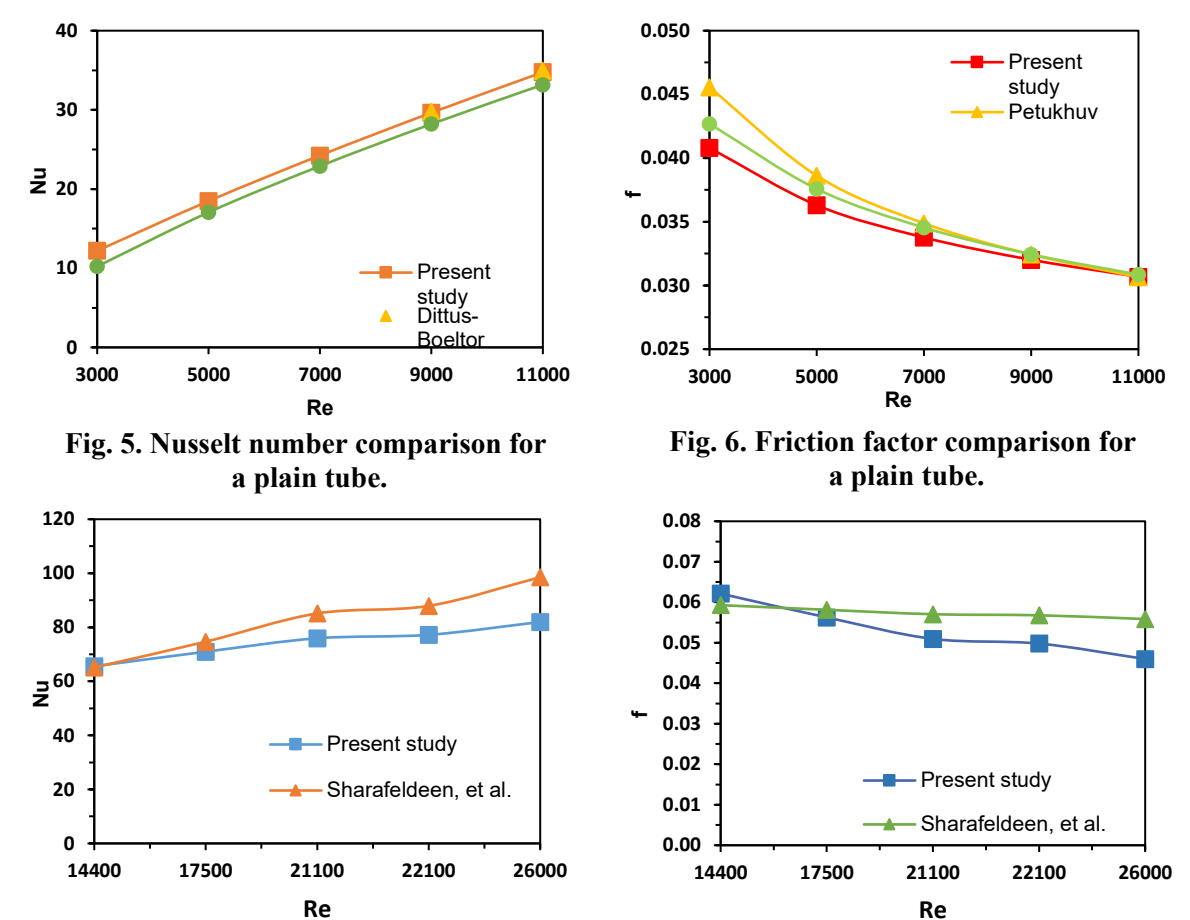


Fig. 7. Nusselt number comparison for a plain tube equipped with a typical circular helical wire.

Fig. 8. Friction factor comparison for a plain tube equipped with a typical circular helical wire.

3. RESULTS AND DISCUSSION

3.1. Velocity contours

For an airflow characterized by a Reynolds number Re = 3000, the results corresponding to axial locations of 0.150, 0.250, 0.350, and 0.450 m, measured from the tube inlet, depicted in frames (a to d), are elucidated in Fig. 9., sequenced from left to right, respectively.

Attributable to the influence of viscosity, the flow velocity within the plain tube (PT) domain, delineated in part (A) of Fig. 9., escalates as it recedes from the tube wall towards its center, culminating in its apex at the center. Concurrently, frames (b to d) of the identical segment

exhibit a congruent pattern of velocity distribution, a consequence of their positioning within the fully developed flow region. Contrarily, frame (a) presents a different pattern, as a result of its location in the developing flow region. The velocity distribution resulting from the insertion of CHCW-NT_7 is displayed in part (B) of Fig. 9, The introduction of the wire induces a swirl flow, disrupting the flow pattern observed in the plain tube. This leads to a more intricate velocity distribution, as shown by the contours. The presence of regions with higher velocity magnitudes is now distributed in the near-wall region, thereby disrupting parts of the boundary layer. Unlike the plain tube, the frames (a to d) of this part display different velocity patterns, which are a result of the absence of fully developed flow and the enhancement of flow mixing. Generally, the insertion of CHCW-NT_1_7_10, and the resulting swirl flow, causes the flow to change the location and distribution of its maximum velocity from one section to another, thereby enhancing flow mixing. In the scenario where models CHCW-NT_10, there is no near wall high velocity spots formulated due to the present of hollow region in the center of tube effected by the high value of R1, resulting in bad mixing.

3.2. Temperature contours

This section investigates the temperature variation across the domain. Fig. 10. presents this

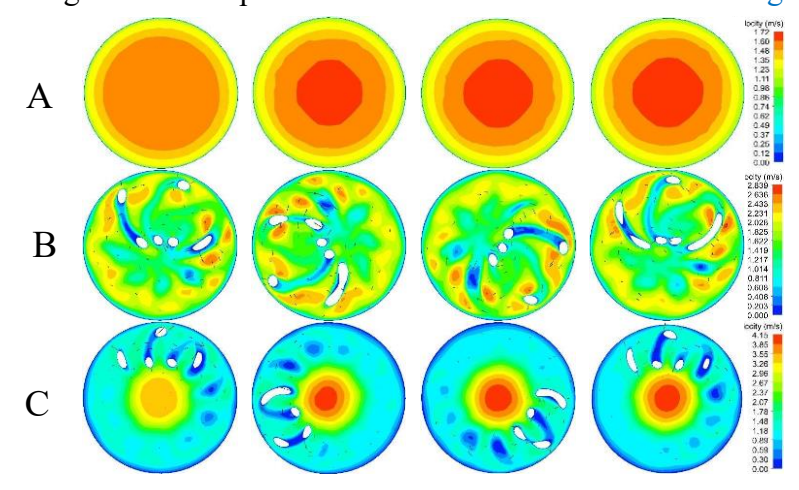


Fig. 9. Velocity Contour overlaid with velocity vectors for; PT (A), CHCW-NT 7 (B), CHCW-NT 10 (C).

variation in contour forms at axial locations same of those of the velocity contours with the same Rynold number. Part (A) pertaining to the Plain Tube (PT), the fluid temperature exhibits a radial increase from the center towards the tube wall, forming a circular pattern. This is attributed to the absence of a swirling flow. As the fluid progresses downstream from the initial location of 0.150 m from the entrance, frame (a), to the locations of 0.250 and 0.350m, frames (b and c), there is a noticeable increase in its temperature. This rise in temperature results in the contraction of the colder region situated at the tube center, due to the escalating heat absorption by the fluid from the tube wall and the expansion of the thermal boundary layer. Consequently,

frame (d) of this part demonstrates a continuous increase in the temperature of the central flow region at downstream locations, owing to the same factors. The influence of the insertion of the CHCW-NT_7, CHCW-NT_10 models on the temperature distribution is demonstrated in Parts B, and C of Fig. 10., respectively. The incorporation of these models transforms the temperature distribution seen in the plain tube case into a star-shaped region, influenced by the wire's projection view along the flow direction, eliminating the circular pattern and pushing the colder region towards the tube wall due to the swirling flow. Similar to the PT, the fluid's high-temperature spots become largest as it travels further downstream inside the tube equipped with CHCW-NT_7, as depicted in the frames of Part (B). A bad mixing behavior discovered in the velocity contours for the model CHCW-NT_7 is present in the thermal performance of this model, thus, the temperature distribution still not disrupted even in the downstream region.

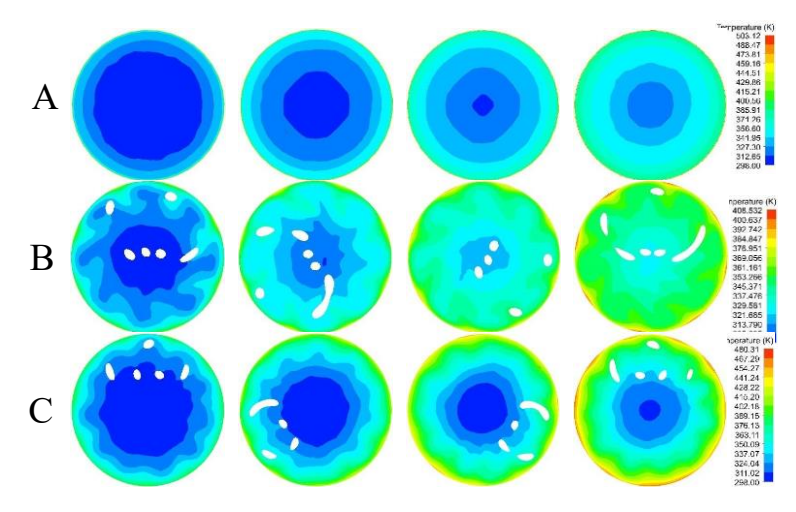


Fig. 10. Temperature contour for; PT (A), CHCW-NT 7 (B), CHCW-NT_10 (C).

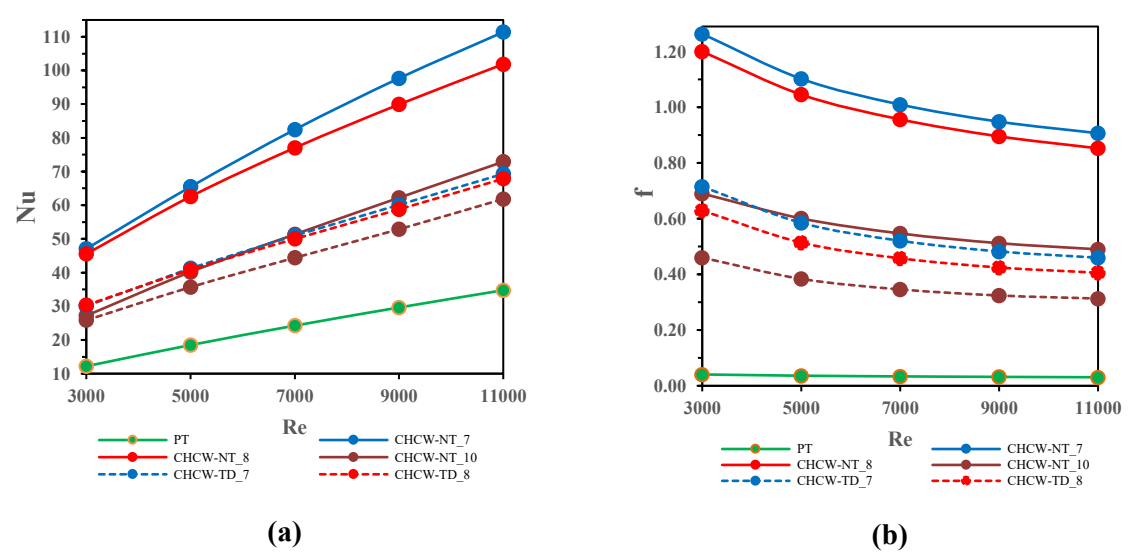


Fig. 11. (a) Average Nusselt number; (b) Friction factor. Corresponding to a tube equipped with helical coiled wires, and plain tube.

3.3. Nusselt number

In Fluent, the fluid's overall bulk temperature is determined through a volume integral using a mass-weighted average, as described below;

$$T_{b} = \frac{\int T_{i} \rho \, dV_{i}}{\int \rho \, dV_{i}} = \frac{\sum_{i=1}^{n} T_{i} \, \rho \, |V_{i}|}{\sum_{i=1}^{n} \rho \, |V_{i}|}$$
(6)

The average surface temperature is calculated through a surface integral using an area-weighted average;

$$T_{s} = \frac{1}{A} \int T_{i} dA_{i} = \frac{1}{A} \sum_{i=1}^{n} T_{i} |A_{i}|$$
 (7)

Now, the coefficient of heat transfer can be calculated by selecting the obtained T_b and T_s in the equation below;

$$h = \frac{q''}{T_S - T_b} \tag{8}$$

Then, the overall Nusselt number based on hydraulic diameter, can be calculated as;

$$Nu = \frac{hD}{k} \tag{9}$$

Where; q'', k, and D are the heat flux, fluid conductivity, and the diameter of plain tube, respectively.

The influence of utilizing a plain tube and the configurations of the studied cases on the average Nusselt number at various Reynolds numbers is elucidated in Fig. 11.(a). As depicted in the illustration, the average Nusselt number exhibits an ascending trend with an increase in Reynolds number across all cases. This behavior can be attributed to the cumulative impact of heightened flow inertia forces arising from alterations in velocity and direction induced by the introduction of helical coiled wires. Furthermore, the figure underscores that the incorporation of any type of helical coiled wire model results in a higher Nusselt number compared to that of a plain tube. This attributed to the generation of swirling flow patterns facilitated by the presence of the helical coiled wire. The discernible rise in the Nusselt number signifies the augmented convective heat transfer efficiency associated with the implementation of helical coiled wire configurations within the studied Reynolds number range. The Nusselt number results for THCW-NT_7 demonstrate the most significant enhancement, reaching 3.86 to 3.2, followed by THCW-NT_8 with a range of 3.73 to 2.93.

3.4. Friction factor

The overall Darcy friction factor was calculated by the relation below:

$$f = \frac{\Delta P}{\frac{1}{2} \rho u_{mean.}^2} \frac{D}{L}$$
(10)

Where:

$$\Delta P = P_{in} - P_{out} \tag{11}$$

 P_{in} was calculated by surface integral by means of area weighted average:

$$P = \frac{1}{A} \int P_i \, dA_i = \frac{1}{A} \sum_{i=1}^n P_i \, |A_i| \tag{2}$$

And P_{out} was specified as boundary condition and was selected as zero Pascal.

The overall mean velocity of fluid is calculated in Fluent by volume integral by means of mass weighted average:

$$u_{mean} = \frac{\int u_{i} \rho \, dV_{i}}{\int \rho \, dV_{i}} = \frac{\sum_{i=1}^{n} u_{i} \, \rho \, |V_{i}|}{\sum_{i=1}^{n} \rho \, |V_{i}|}$$
(13)

While the presence of insertions can augment the Nusselt number, indicating enhanced heat transfer, this often comes with a trade-off in the form of an increased pressure drop. This increase is typically represented by the friction factor (Mohammed G. Jehad, 2010). Fig. 11.(b) illustrates the friction factor for turbulent airflow in both a plain tube and a tube equipped with the studded models at different Reynolds numbers. The figure shows a decreasing trend in the friction factor as the Reynolds number increases in all the scenarios studied. This is due to the simultaneous increase in velocity that accompanies the rise in Reynolds number. Furthermore, the figure emphasizes that the models THCW-NT_7, and THCW-NT_8 display higher friction factors compared to other models.

3.5. Thermal performance factor (TPF)

The thermal performance factor (TPF) is a critical parameter. This factor was computed utilizing Eq.1, proposed by (Webb, 1981):

$$TPF = (Nu / Nu_p) / (f / f_p)^{-1/3}$$
(14)

The relationship between the TPF and the Reynolds number for the studied scenarios is graphically represented in Fig. 12. This graphical representation clearly indicates an inverse relationship between the Reynolds number and the TPF. Among the various models studied, the model designated as CHCW-NT_7, demonstrated a superior TPF within all Reynolds number ranges ranged from 1.228 to 1.036, followed by THCW-NT_8 ranged from 1.209 to 0.968.

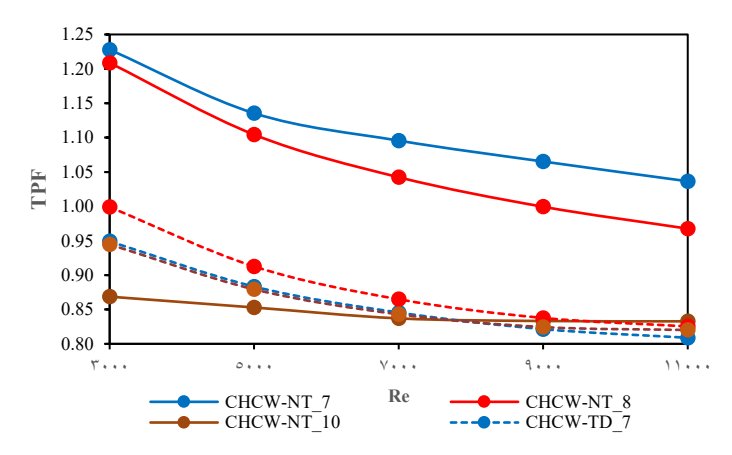


Fig. 12. Thermal performance factor Corresponding to a tube equipped with helical coiled wires.

4. CONCLUSIONS

The numerical investigation for utilization HCWs as turbulence promoters, aiming to elucidate their impact on both thermal and hydro-dynamic fields. Based on the endeavors undertaken and the results obtained, it can be deduced that; the Nusselt number ratio, friction factor ratio and thermal performance factor all show a decrease as the Reynolds number increases. At a pitch ratio of (P/D) = 1, large base radius (R1) = 7 mm, coiled wire pitch (p) = 6 mm, and Re = 3000, the helical coiled wire achieved the maximum TPF of 1.228, highest augmentation in the Nusselt number and highest increasing in friction factor.

The utilization of helical coiled wire as a turbulent promoter for both circular and triangular cross-section wires signifies a fresh field of research. To the author's best understanding, the employment of such a promoter has not been documented in open-access literature. As such, this study can serve as a pioneering effort to delve into the study of these types of promoters. In consideration of this, the subsequent recommendations can be put forth:

- The present study focused on circular wire cross-sections. future research could investigate the effects of other geometric configurations, such as triangular, square, rectangular, or even more complex cross-sectional shapes. The impact of these different shapes on heat transfer and turbulence could provide additional insights into the optimization of the system. Another interesting area of research could be the combination of different cross-sectional shapes in the same helical coil. This could involve alternating between circular and triangular sections, or using a different shape entirely. The resulting effects on heat transfer and turbulence could be quite unique and worth investigating.
- The tapering ratio, which remained constant in the current study, could be varied in the next stage to study its effect on thermal performance.

- The clearance, another factor that was held constant, could be altered to understand its influence on the system's thermal performance.
- The Reynolds number ranges tested in the present study could be expanded in the future studies. This could involve testing lower or higher Reynolds number ranges to see how they affect the thermal performance of the model.

5. REFERENCES

Abd zaid, D.N., & Hamzah, D.A. (2021), "Heat Transfer Enhancement by Turbulence Generator inside Heat Receiver", Al-Qadisiyah Journal for Engineering Sciences, 13(4), pp.268-273. https://doi.org/10.30772/qjes.v13i4.680.

Aldawi, F. (2022), "Novel validated numerical analysis of flat coil tube with spring inserts", Case Studies in Thermal Engineering, 36, p.102197. https://doi.org/10.1016/j.csite.2022.102197.

Bochenek, B., & Ustrnul, Z. (2022), "Machine Learning in Weather Prediction and Climate Analyses—Applications and Perspectives", Atmosphere, 13(2), p.180. https://doi.org/10.3390/atmos13020180.

Chang, S.W., Gao, J., & Shih, H.P. (2015), "Thermal performances of turbulent tubular flows enhanced by ribbed and grooved wire coils", International Journal of Heat and Mass Transfer, 90, pp.1109-1124. https://doi.org/10.1016/j.ijheatmasstransfer.2015.07.070.

Dang, W., & Wang, L.-B. (2021), "Convective heat transfer enhancement mechanisms in circular tube inserted with a type of twined coil", International Journal of Heat and Mass Transfer, 169, p.120960. https://doi.org/10.1016/j.ijheatmasstransfer.2021.120960.

Dhumal, A.R., Kulkarni, A.P., & Ambhore, N.H. (2023), "A comprehensive review on thermal management of electronic devices", Journal of Engineering and Applied Science, 70(1). https://doi.org/10.1186/s44147-023-00309-2.

Dostál, M., Petera, K., & Solnař, S. (2022), "Gnielinski's correlation and a modern temperature-oscillation method for measuring heat transfer coefficients", EPJ Web of Conferences, 269, p.01009. https://doi.org/10.1051/epjconf/202226901009.

Du, J., Hong, Y., Wang, S., Ye, W., & Huang, S.-M. (2018), "Experimental thermal and flow characteristics in a traverse corrugated tube fitted with regularly spaced modified wire coils", International Journal of Thermal Sciences, 133, pp.330-340. https://doi.org/10.1016/j.ijthermalsci.2018.05.032.

García, A., Herrero-Martin, R., Pérez-García, J., & Solano, J.P. (2023), "Validation of a new methodological approach for the selection of wire-coil inserts in thermal equipment", Applied Thermal Engineering, 218, pp.119273-119273. https://doi.org/10.1016/j.applthermaleng.2022.119273.

García, A., Solano, J.P., Vicente, P.G., & Viedma, A. (2012), "The influence of artificial roughness shape on heat transfer enhancement: Corrugated tubes, dimpled tubes and wire coils", Applied Thermal Engineering, 35, pp.196-201. https://doi.org/10.1016/j.applthermaleng.2011.10.030.

Ghassan Fadhil Smaisim (2018), "AUGMENTATION OF HEAT TRANSFER IN CORRUGATED TUBE USING FOUR-START SPIRAL WALL", Al-Qadisiyah Journal for Engineering Sciences, 10(4). https://doi.org/10.30772/qjes.v10i4.493.

Göksu, T.T., & Yılmaz, F. (2021), "Numerical comparison study on heat transfer enhancement of different cross-section wire coils insert with varying pitches in a duct", Journal of Thermal Engineering, 7(7), pp.1683-1693. https://doi.org/10.18186/thermal.1025930.

Hinge, S.P., & Patwardhan, A.W. (2019), "Thermal-Hydraulic Performance of an Annular Pipe with Square Wire Coil Inserts Using Computational Fluid Dynamics", Industrial & Engineering Chemistry Research, 59(9), pp.3887-3903. https://doi.org/10.1021/acs.iecr.9b04192.

Hussien, D., Kassim, M., & Yousif, M. (2023), "Numerical study of effect porous media on heat transfer in a horizontal annular tube", Al-Qadisiyah Journal for Engineering Sciences, 16(4), pp.292-300. https://doi.org/10.30772/qjes.2023.143069.1028.

Keklikcioglu, O., & Ozceyhan, V. (2022), "Heat transfer augmentation in a tube with conical wire coils using a mixture of ethylene glycol/water as a fluid", International Journal of Thermal Sciences, 171, pp.107204-107204. https://doi.org/10.1016/j.ijthermalsci.2021.107204.

Kumar, R., Chandra, P., & Singh, H. (2023), "Experimental Analysis of Heat Transfer in a Triple Tube Heat Exchanger with Spring Turbulator Using CuO/Water Nanofluid", Journal of Nanofluids, 12(2), pp.429-437. https://doi.org/10.1166/jon.2023.1936.

Mohammed G. Jehad (2010), "EXPERIMENTAL STUDY OF THE FRICTION FACTOR IN EQUILATERAL TRIANGULAR DUCT WITH DIFFERENT TYPES OF VOREX GENERATORS (OBSTACLES)", Al-Qadisiyah Journal for Engineering Sciences, vol. 3, no. 2, pp. 161-172.

Oehlschlaeger, M.A. (2022), "Grand challenges in aerospace propulsion", Frontiers in Aerospace Engineering, 1. https://doi.org/10.3389/fpace.2022.1027943.

San, J.-Y., Huang, W.-C., & Chen, C.-A. (2015), "Experimental investigation on heat transfer and fluid friction correlations for circular tubes with coiled-wire inserts", International Communications in Heat and Mass Transfer, 65, pp.8-14. https://doi.org/10.1016/j.icheatmasstransfer.2015.04.008.

Sharafeldeen, M.A., Berbish, N.S., Moawed, M.A., & Ali, R.K. (2016), "Experimental investigation of heat transfer and pressure drop of turbulent flow inside tube with inserted helical coils", Heat and Mass Transfer, 53(4), pp.1265-1276. https://doi.org/10.1007/s00231-016-1897-z.

Sharifi, K., Sabeti, M., Rafiei, M., Mohammadi, A.H., Ghaffari, A., Asl, M.H., & Yousefi, H. (2020), "A good contribution of computational fluid dynamics (CFD) and GA-ANN methods to find the best type of helical wire inserted tube in heat exchangers", International Journal of Thermal Sciences, 154, p.106398. https://doi.org/10.1016/j.ijthermalsci.2020.106398.

Taler, D. (2017), "Simple power-type heat transfer correlations for turbulent pipe flow in tubes", Journal of Thermal Science, 26(4), pp.339-348. https://doi.org/10.1007/s11630-017-0947-2.

Wang, L., & Zhang, X.-R. (2023), "Industrial Cooling Systems", Lecture notes in energy, pp.313-336. https://doi.org/10.1007/978-3-031-22512-3 10.

Webb, R.L. (1981), "Performance evaluation criteria for use of enhanced heat transfer surfaces in heat exchanger design", International Journal of Heat and Mass Transfer, 24(4), pp.715-726. https://doi.org/10.1016/0017-9310(81)90015-6.

Yang, Y., Li, M., Zou, Y., & Chen, J. (2021), "Numerical study on heat transfer characteristics of molten salt in annular channel with wire coil", Applied Thermal Engineering, 199, p.117520. https://doi.org/10.1016/j.applthermaleng.2021.117520.

Yin, P., Hasan, Y.M., Bashar, B.S., Zahra, A., Radhy, M., Majed, H., Alhani, I., Abood, E.S., Hadrawi, S.K., Alizadeh, A., & Hekmatifar, M. (2023), "Evaluation of efficiency, thermohydraulic performance evaluation criterion, and field synergy principle improvement of the parabolic solar collector containing the hybrid nanofluid using spring turbulators", Case Studies in Thermal Engineering, 41, pp.102571-102571. https://doi.org/10.1016/j.csite.2022.102571.

Yu, C., Zhang, H., Wang, Y., Zeng, M., & Gao, B. (2020), "Numerical study on turbulent heat transfer performance of twisted oval tube with different cross sectioned wire coil", Case Studies in Thermal Engineering, 22, pp.100759-100759. https://doi.org/10.1016/j.csite.2020.100759.

Zimparov, V., Bonev, P., Angelov, M., & Hristov, J. (2022), "Benefits from the use of wire-coil inserts in water transitional and low turbulent flow: The influence of the wire-coil pitch", Thermal Science, 26(4 Part B), pp.3597-3604. https://doi.org/10.2298/tsci211206060z.